ARTICLE

BIOTECHNOLOGY and BIOENGINEERING

Specific Growth Rate and Multiplicity of Infection Affect High-Cell-Density Fermentation With Bacteriophage M13 for ssDNA Production

Benjamin Kick,[1] Samantha Hensler,[1] Florian Praetorius,[2] Hendrik Dietz,[2] Dirk Weuster-Botz[1]

[1]Institute of Biochemical Engineering, Technical University of Munich, Boltzmannstr. 15, Garching 85748, Germany; telephone: +49-89-28915712; fax: + 49-89-28915714; e-mail: d.weuster-botz@lrz.tum.de

[2]Physik Department and Institute for Advanced Study, Technical University of Munich, Garching, Germany

ABSTRACT: The bacteriophage M13 has found frequent applications in nanobiotechnology due to its chemically and genetically tunable protein surface and its ability to self-assemble into colloidal membranes. Additionally, its single-stranded (ss) genome is commonly used as scaffold for DNA origami. Despite the manifold uses of M13, upstream production methods for phage and scaffold ssDNA are underexamined with respect to future industrial usage. Here, the high-cell-density phage production with *Escherichia coli* as host organism was studied in respect of medium composition, infection time, multiplicity of infection, and specific growth rate. The specific growth rate and the multiplicity of infection were identified as the crucial state variables that influence phage amplification rate on one hand and the concentration of produced ssDNA on the other hand. Using a growth rate of 0.15 h^{-1} and a multiplicity of infection of 0.05 pfu cfu^{-1} in the fed-batch production process, the concentration of pure isolated M13 ssDNA usable for scaffolded DNA origami could be enhanced by 54% to 590 mg L^{-1}. Thus, our results help enabling M13 production for industrial uses in nanobiotechnology.

Biotechnol. Bioeng. 2016;9999: 1–8.

KEYWORDS: Bacteriophage M13; high-cell-density fermentation; single-stranded DNA; DNA origami; *Escherichia coli*

Conflict of interest: The authors have declared no conflict of interest.
Correspondence to: D. Weuster-Botz
Contract grant sponsor: Deutsche Forschungsgemeinschaft (DFG)
Contract grant sponsor: TUM International Graduate School of Science and Engineering (IGSSE)
Contract grant sponsor: Excellence Cluster Center for Integrated Protein Science
Contract grant sponsor: Nano Initiative Munich
Contract grant sponsor: Sonderforschungsbereich
Contract grant number: SFB863
Contract grant sponsor: European Research Council
Contract grant number: t256270
Received 29 July 2016; Revision received 30 September 2016; Accepted 10 October 2016
Accepted manuscript online xx Month 2016;
Article first published online in Wiley Online Library (wileyonlinelibrary.com).
DOI 10.1002/bit.26200

Introduction

Since the discovery of the bacteriophage M13 in 1963 by Hofschneider, this virion was used to develop molecular biology tools and to further understand gene regulation. Due to its simple structure, with a single-stranded genome coding for 11 proteins, it is an attractive vehicle, for example, used as cloning vector or for phage display technologies (Hofschneider, 1963; Rakonjac et al., 2011). More recently, the bacteriophage M13 has emerged as a powerful tool in nanobiotechnology, owing to the genetically and chemically alterable protein surface and the ability to form colloidal membranes (Sharma et al., 2014). Bacteriophage M13 applications range from—but are not limited to—nanotemplates for organic and inorganic modifications (Bernard and Francis, 2014), nanoscale electrical material for lithium-ion batteries (Lee et al., 2009; Moradi et al., 2015; Whaley et al., 2000), biofuel cells (Blaik et al., 2016), and biomimetic self-templating structures (Chung et al., 2011) to colorimetric sensors (Oh et al., 2014). In addition to applications in nanobiotechnology, the bacteriophage M13 showed powerful potential in the disaggregation of misfolded proteins, for example, alpha-synuclein. According to the predominant hypothesis today, the deposition of polymerized synuclein is an indicator for Parkinson's disease (Dimant et al., 2009; Messing, 2016).

Furthermore, the ssDNA genome of bacteriophage M13 is commonly used as scaffold for the so-called "scaffolded DNA origami" technology (Rothemund Paul, 2006). In this bottom-up method, the long scaffold ssDNA strand and a set of short "staple" oligonucleotides self-assemble into user-defined two- or three-dimensional shapes. Application of these nanostructures as alignment media in NMR spectroscopy (Berardi et al., 2011), as nanopores in lipid membranes (Burns et al., 2016; Langecker et al., 2012) and as drug delivery systems (Douglas et al., 2012; Yan et al., 2015) or as nanomachines (Ketterer et al., 2016), have already been shown or are conceivable in the future. However, applications of DNA origami ultimately depend on the availability of scaffold ssDNA in good quality and high quantities.

The bacteriophage M13 infects male *Escherichia coli* (*E. coli*) cells by attaching to the F-pilus and injecting its ssDNA genome into the host. Intracellularly, the ssDNA is converted into the double-stranded replicative form (RF) by bacterial enzymes. The RF DNA serves as template for the transcription of the phage genes and rolling circle ssDNA amplification (Henry and Pratt, 1969; Schröder et al., 1973). During assembly of phage coat protein and ssDNA genome, the phage is secreted through the cell membrane without lysis of the host cell.

Large-scale utilization of bacteriophage in material science, pharmaceutical applications or as ssDNA scaffold for DNA origami requires investigation to enable industrial usage. Progress was achieved by Branston et al. (2011) concerning the robustness of filamentous bacteriophage M13 for large-scale processing. Recently, a new technology was developed for endotoxin removal from bacteriophages for pharmaceutical applications (Branston et al., 2015). Despite these improvements, the fermentation process with bacteriophage M13 is hardly studied in bioreactors.

Recently, a fed-batch process was described for the production of scaffold ssDNA with bacteriophage M13 in a lab-scale stirred-tank bioreactor, upgrading the scale of produced ssDNA from the milligram to the gram (Kick et al., 2015). Nevertheless, the limiting state variables for achieving high ssDNA concentrations remained unclear. These may include medium components or produced byproducts, as well as specific growth rate in combination with the time and multiplicity of infection.

Materials and Methods

Bacterial Strain, Bacteriophage M13, and Medium Preparation

An *E. coli* XL1-Blue MRF' Kan^+ strain (Δ(mcrA)183 Δ(mcrCB-hsdSMR-mrr)173 endA1 supE44 thi-1 recA1 gyrA96 relA1 lac [F' proAB lacIqZΔM15 Tn5 (Kanr)]) (Stratagene) was used as host organism. Stock suspensions of bacteriophage M13mp18 and variants in ssDNA genome length (Douglas et al., 2009), medium and preculture preparation were performed as described previously (Kick et al., 2015). To accomplish variation in multiplicity of infection, phage suspensions were used with titers up to 10^{14} pfu mL^{-1}, which were produced in a fed-batch process.

Bioreactor, Fermentation Process, and Feeding Solution

All fermentations were carried out in a stirred-tank bioreactor with two 6 plate Rhuston turbines (KLF Advanced System 3.6 L, Bioengineering AG, Wald, Switzerland) using 1.6 L defined basal medium according to Riesenberg et al. (1991), with a batch glucose concentration of 25 g L^{-1}, 1 mM Thiamin-HCl, and 50 mg L^{-1} Kanamycin A at 37°C. A pH of 6.7 was maintained with 25% NH_4OH. If required, 0.1% v/v antifoam solution (Antifoam 204, Sigma–Aldrich, Taufkirchen, Germany) was added autonomously during fermentation after response of the antifoam probe in the reactor headspace. The dissolved oxygen concentration was controlled at 25% air saturation at 2 vvm sterile air flow by increasing the stirrer speed and pressure up to 1,500 rpm and 2.0 bar, respectively. Exponential growing cells from shake flasks without baffles were concentrated and resuspended in 20 mL Riesenberg basal medium to inoculate the bioreactor. If not mentioned otherwise, a glucose limiting exponential feeding phase was applied with a predefined specific growth rate of 0.15 h^{-1}, which started after depletion of the batch glucose. The exponential feeding lasted 12.5 h up to maximal 20.7 g_{Glc} L^{-1} h^{-1}, followed by a linear decrease for 1.5 h until the constant glucose mass flow rate of 7.7 g_{Glc} L^{-1} h^{-1} was reached. The exponential feeding phase was designed with the following simplified equation ignoring substrate consumption for maintenance and increase of reaction volume:

$$\dot{V} = \frac{1}{c_{S0}} \left(\frac{\mu_{set}}{Y_{XS,\mu}} \right) c_{X0} e^{\mu_{set}(t-t_0)} V$$

where $\dot{V}$ denotes the volumetric flow rate, c_{S0} the substrate concentration in the feed, μ_{set} the specific growth rate, $Y_{XS,\mu}$ the biomass yield, c_{x0} the biomass at the end of batch phase, t the time after feeding started, and V the reaction volume at the end of batch phase. The volume specific mass flow of glucose was calculated using the glucose concentration and the actual reaction volume. The feeding solution consisted of 750 g L^{-1} glucose, 20 g L^{-1} $MgSO_4 \cdot 7\ H_2O$, and 18.5 g L^{-1} $(NH_4)_2SO_4$, if not mentioned otherwise. Criteria were defined to design comparable experiments with varying specific growth rate: first, the exponential feeding profile was terminated at a cell concentration of 60 g L^{-1}. Secondly, the total amount of glucose fed into the reactor was fixed to 572 g. To achieve a comparable process time at the growth rate of 0.1 h^{-1}, the constant feeding rate was increased to 11.1 g_{Glc} L^{-1} h^{-1}.

The downstream processing of ssDNA was performed as described recently (Kick et al., 2015) after every fed-batch process to analyze quantity and quality of the isolated ssDNA.

Analytic Methods

The cell growth was determined at-line by measurement of optical density at 600 nm (Genesys 10S UV–VIS, Thermo Fisher Scientific Inc., Waltham, MA). The cell dry weight was measured offline by centrifugation (13,000 rcf, 10 min) and drying until constant weight of 2 mL culture broth. Concentration of glucose, ammonium, acetate, magnesium, and phosphate were measured in the supernatant after cell removal using enzymatic or colorimetric assays according to vendors instructions (D-glucose: 10 716 251 035, ammonium: 11 112 732 035, acetate: 10 148 261 035 R-Biopharm AG, Darmstadt, Germany, magnesium: MF01000100-2, Centronic GmbH, Wartenberg, Germany, phosphate: MAK030-1KT, Sigma–Aldrich, Taufkirchen, Germany). The direct plating plaque assay was used to carry out the enumeration of bacteriophages in the supernatant (Clokie and Kropinski, 2009). The phage amplification rate was calculated using the decadic logarithm of the phage titer. The sigmoidal behavior of the phage titer progress (decadic logarithm) was fitted using nonlinear regression over the whole period after phage addition (Sigma Plot 12.5, Systat Software)

according to

$$y(t) = y_0 + \frac{a}{1 + \exp\left(-\frac{(t-c)}{b}\right)}$$

where y_0 is the decadic logarithm of the phage titer at time of infection, a, b, and c are fitted coefficients. The slope of the approximated curve was defined as phage amplification rate. The uncertainty of the phage amplification rate was estimated by error propagation of the 95% confidence interval of the approximated phage titer progress.

For the offline analytic of ssDNA concentration, the ssDNA genome of bacteriophage was isolated on a milliliter scale. To separate cells and phages, 2 mL fermentation broth was centrifuged for 10 min and 13,000 rcf at 20°C (Espresso Microcentrifuge, Thermo Fisher Scientific Inc.). By addition of 72 mg polyethylene glycol and 54 mg sodium chloride the phages were precipitated for 30 min at room temperature. After centrifugation (10 min, 13,000 rcf, 20°C) the precipitated phages were resuspended in 200 µL TE-buffer (10 mM Tris HCL, 1 mM EDTA, pH 8.5). The phages were lysed by addition of 400 µL lysis buffer (200 mM NaOH, 1% SDS, 1 min) and 300 µL neutralization buffer (3 M potassium acetate, pH 5.5) and subsequently chilled on ice for 15 min. The supernatant (10 min, 13,000 rcf, 20°C) containing ssDNA was mixed with 900 µL chilled ethanol (99%, −20°C) and incubated for 30 min on ice. The precipitated ssDNA (10 min, 13,000 rcf, 20°C) was again washed with ethanol (75%, −20°C, 10 min) and centrifuged afterward. The supernatant was completely discarded and the precipitated ssDNA was solved and diluted in TE-buffer. The fluorescent stain SYBR® Gold nucleic acid (Thermo Fisher Scientific Inc.) in black µClear® MTPs (Greiner-Bio-One GmbH, Frickenhausen, Germany) was used for ssDNA quantification with excitation at 495 nm and emission at 550 nm. The fluorescent intensity was measured with a MTP reader (Tecan Infinite® M200, Tecan, Crailsheim, Germany), with a linearity in the range of 0.01–0.5 nM using M13mp18 ssDNA as reference. Quality control of purified ssDNA was performed using agarose gel electrophoresis as previously described (Kick et al., 2015). The concentration of ssDNA was normalized before loading the gel. The migration analysis of agarose gel electrophoresis was performed with purified, coiled ssDNA diluted in TE-buffer.

Results and Discussion

Medium Composition

During fed-batch fermentation with bacteriophage infection the amount of biomass produced was significantly lower compared to host cell fermentation. Without phage infection, cell dry weights of 93 g L^{-1} were achieved, whereas the maximal cell dry weight was 65 g L^{-1} with phage production (Fig. 1A). This implies a possible medium limitation in fed-batch process due to differences in cell metabolism after phage infection. We analyzed the medium

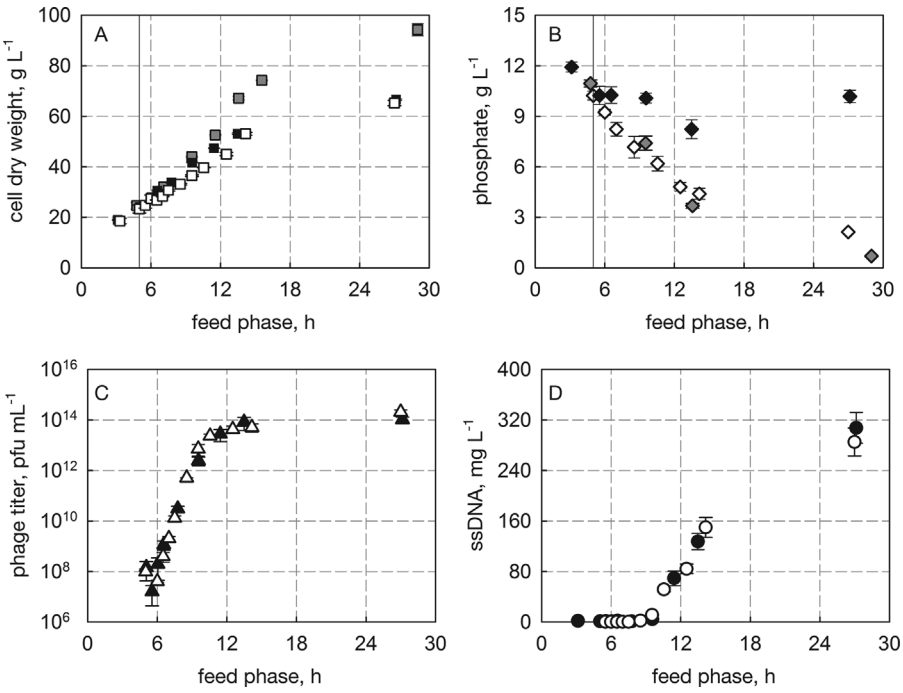

Figure 1. Additional phosphate feeding during high-cell-density fermentation. Fed-batch fermentation of *E. coli* XL1-blue MRF' was performed without phage infection (gray symbols), with phage infection (white symbols), and with additional $(NH_4)_2HPO_4$ feeding (0.35 $g_{Phosphate}$ L^{-1} h^{-1}) (black symbols). The cell dry weights (**A**), the phosphate concentrations (**B**), the phage titers (**C**), and the isolated ssDNA (**D**) are plotted against process time in the feed phase. The vertical line indicates the time of infection and the start of additional phosphate feeding.

components ammonium, magnesium, phosphate, and acetate as possible byproduct, beneath the limiting substrate glucose. Owing to the glucose limiting feed profile and the sufficient oxygen supply, the acetate concentration was below 0.01 g L^{-1} at any time. The concentration of ammonium and magnesium was never limiting or inhibiting, referring to the literature data for ammonium (<3.0 g L^{-1}) and magnesium (<8.7 g L^{-1}) for the fermentation of *E. coli* (Lee, 1996; Shiloach and Fass, 2005). In contrast, the phosphate concentration decreased drastically in the fed-batch process from 10.9 to 0.7 g L^{-1} (Fig. 1B). Applying an additional phosphate feeding of 0.35 $g_{Phosphate}$ L^{-1} h^{-1} ($(NH_4)_2HPO_4$), the phosphate concentration was kept above 8 g L^{-1} at any time. Nevertheless, this revealed no positive effect regarding biomass or phage or ssDNA concentration (Fig. 1C and D).

But the phosphate source seems to be a crucial parameter influencing ssDNA quality. The fed-batch experiments performed with KH_2PO_4 instead of $(NH_4)_2HPO_4$ as additional phosphate source, yielded lower quality of isolated ssDNA (Fig. 2). The presence of impurities and, thus, a lower quality of the ssDNA in lane 1 is represented by higher intensities in the area above the leading band, especially in the pocket (Fig. 2).

Anderson et al. (1975) described a dissociation of the protein P5 and ssDNA complex at concentrations of 0.1 M divalent or 0.5 M monovalent cations in vitro. In the M13 phage life cycle, the P5 and ssDNA complex prevents the conversion into the replicative form (RF) (Stassen et al., 1995). Subsequently, the P5 protein is replaced by phage coat protein P8 during extrusion through the cell membrane. The additional KH_2PO_4 feeding resulted in a 50% increase in potassium concentration to a theoretical maximal of 0.3 M at the end of the fed-batch process. Although the used Riesenberg medium contained KH_2PO_4, the alteration of one single medium component reduced the ssDNA quality. This demonstrates the sensitivity of the whole process regarding medium composition. Nevertheless, any medium limitation was excluded in the fed-batch process due to the analysis of medium components and the addition of $(NH_4)_2HPO_4$ as additional phosphate source.

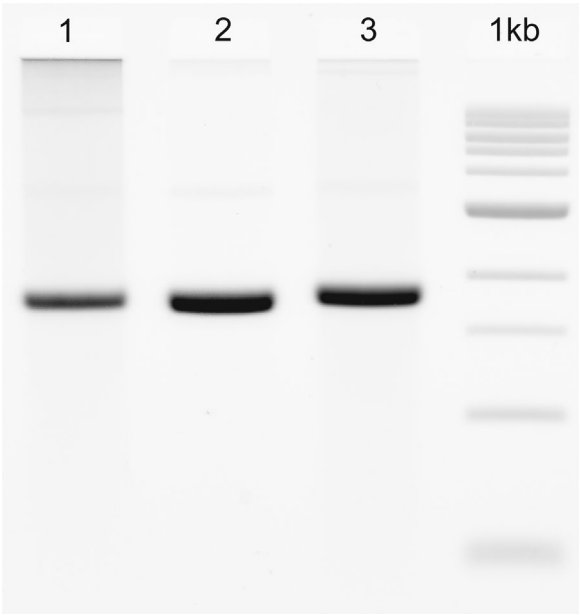

Figure 2. Influence of phosphate source on ssDNA quality. Image of an agarose gel containing ssDNA samples from fed-batch experiments with KH_2PO_4 (**1**), without additional phosphate (**2**), and with $(NH_4)_2HPO_4$ (**3**). Lane 1 shows higher intensities in the area above the leading band, indicating the presence of impurities and thus lower quality of the ssDNA. Differences in the migration distance of the leading band can be attributed to the difference in length between the ssDNA samples (7249 bases in 1 and 2, 7560 bases in 3).

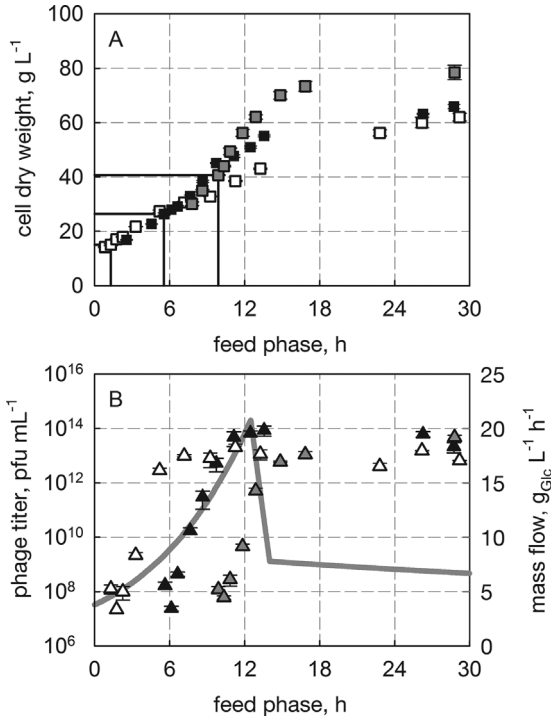

Figure 3. Cell dry weight and phage titer as function of time of infection. Fed-batch phage fermentations were carried out with infection at a cell dry weight of 15 g L^{-1} (white symbols), 26 g L^{-1} (black symbols), and 40 g L^{-1} (gray symbols). The cell dry weights (**A**), the phage titers and the glucose mass flow (**B**) are shown.

Time of Infection

Infection with bacteriophage M13 was performed at different cell densities (15, 26, and 40 g L^{-1}, respectively) during the exponential feeding phase with an averaged multiplicity of infection (MOI) of 0.0025 ± 0.0012 pfu cfu^{-1} (Table I). Applying a poisson distribution, the proportion of cells infected with at least one phage can be calculated using the MOI (Ellis and Delbrück, 1938). At the time of infection, a minor proportion of 0.1–0.3% of the cells is theoretically infected. Despite the high standard deviation of the single MOIs, this indicates the comparability of the experiments.

The addition of phages at a dry cell mass concentration of 40 g L^{-1} led to the highest maximal cell dry weight of 80 g L^{-1}, whereas the maximal phage titer reached the same magnitude up to 10^{14} pfu mL^{-1} in comparison to the other infection times (Fig. 3A and B). Furthermore, the maximal phage amplification rate is independent of the time of infection, under the investigated

Table I. Maximal phage amplification rate and final ssDNA concentration in fed-batch processes with varying infection times.

CDW [g L^{-1}]	MOI [pfu cfu^{-1}]	Infected cells at time of infection [%]	Max. phage amplification rate [h^{-1}]	c (ssDNA) [g L^{-1}]	Normalized ssDNA concentration
15.1 ± 0.3	$3.5 \pm 1.2 \cdot 10^{-3}$	0.3 ± 0.1	1.7 ± 0.1	0.24 ± 0.02	0.65
26.4 ± 0.5	$2.9 \pm 0.9 \cdot 10^{-3}$	0.3 ± 0.1	1.5 ± 0.05	0.37 ± 0.03	1.00
40.7 ± 0.2	$1.1 \pm 0.6 \cdot 10^{-3}$	0.1 ± 0.06	1.6 ± 0.09	0.28 ± 0.01	0.76

The proportion of cells infected at time of infection was calculated following a poisson distribution.

conditions (Table I). The phage amplification rate describes the increase of phage titer in magnitudes per hour. For an early infection time, the stagnation in phage amplification rate occurred already during exponential feeding and is thus not caused by the end of exponentially growing cells (Fig. 3). Infection at 26 g L^{-1} after 5 h of exponential feeding resulted in the highest isolated ssDNA amount of 0.37 g L^{-1} (Table I).

In shake flask experiments, the infection was executed at optical densities of 0.5 or below (Douglas et al., 2007; Sambrook et al., 2001). Here, the time of infection at cell dry weights of 15–40 g L^{-1} showed no influence on the phage amplification rates and can be chosen arbitrary. This finding can be attributed to longer substrate supply, higher cell dry weights, and longer process times in fed-batch processes in contrast to batch experiments in shake flasks. Nevertheless, the infection with bacteriophage M13 in the mid phase of exponential feeding gave the highest concentration of isolated ssDNA. In accordance with fed-batch fermentations for heterologous protein expression with *E. coli*, the choice of optimal induction time is important for productivity (Choi et al., 2006).

Specific Growth Rate

To investigate the influence of the specific growth rate of *E. coli* XL1-blue on phage production, different predefined exponential feeding profiles were applied to achieve growth rates between $\mu_{set} = 0.1$–$0.2\,h^{-1}$. To avoid glucose accumulation and acetate formation, the controlled specific growth rate was limited to $\mu_{set} = 0.2\,h^{-1}$ at the maximal, since infected *E. coli* XL1-blue can grow with a maximal growth rate of $0.24\,h^{-1}$ in batch processes with this defined medium (Kick et al., 2015). A slower cell specific growth rate resulted in a higher maximal biomass concentration, although the total fed glucose amount was identical in every fed-batch process (Fig. 4).

The variation of feed profiles revealed that increasing the specific growth rates from 0.1 to $0.2\,h^{-1}$ enhanced the maximal phage amplification rate from 0.7 to $2.2\,h^{-1}$. Furthermore, the lower growth rate led to a longer phage production period, nevertheless yielding a phage titer in the same order of magnitude at the end of the process (Fig. 5A and B).

The isolated ssDNA concentration confirmed a relationship between growth rate and phage production rate. The fed-batch fermentation with the growth rate of $0.2\,h^{-1}$ achieved the maximal cell specific ssDNA formation rate of $1.7\,mg\,g_{CDW}^{-1}\,h^{-1}$ and a volumetric productivity of $74.4\,mg\,L^{-1}\,h^{-1}$. Although the cell specific ssDNA productivity was increased by higher growth rate, the overall amount of ssDNA produced was the same at growth rates of 0.15 and $0.2\,h^{-1}$. Only the lowest growth rate of $0.1\,h^{-1}$ yielded 25% less ssDNA and the highest cell dry weight concentration (Fig. 5C and D). In Figure 6, the phage amplification rate is plotted against the ratio of phage to cell. The maximal values for the phage amplification rate were reached between 0.4 and 1.9 pfu cfu^{-1}, where theoretically 33–85% of the cells were infected with at least one phage according to the poisson distribution (Ellis and Delbrück, 1938).

Although more slowly growing cells produce more phages in batch experiments in shake flasks (Salivar et al., 1964), the fully controlled fed-batch studies in a stirred-tank bioreactor indicate a contrary relationship. To exclude a strain specific behavior between growth rate and phage production rate, another *E. coli* strain (JM 109, data not shown) was studied in the fed-batch process, showing

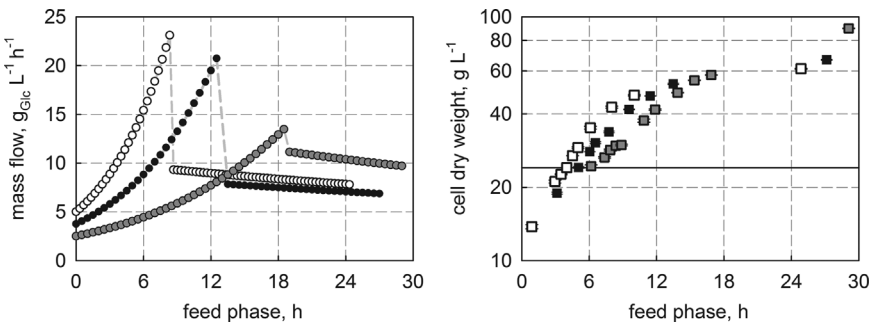

Figure 4. Variation of exponential feeding profiles. Left: The predefined feed profiles with growth rates of $\mu_{set} = 0.2\,h^{-1}$ (white symbols), $0.15\,h^{-1}$ (black symbols), and $0.1\,h^{-1}$ (gray symbols) in the exponential feeding phase are plotted against process time in the feed phase. Right: The cell dry weight is plotted semi-logarithmically against the process time in feed phase. The horizontal line indicates the cell dry weight at phage infection.

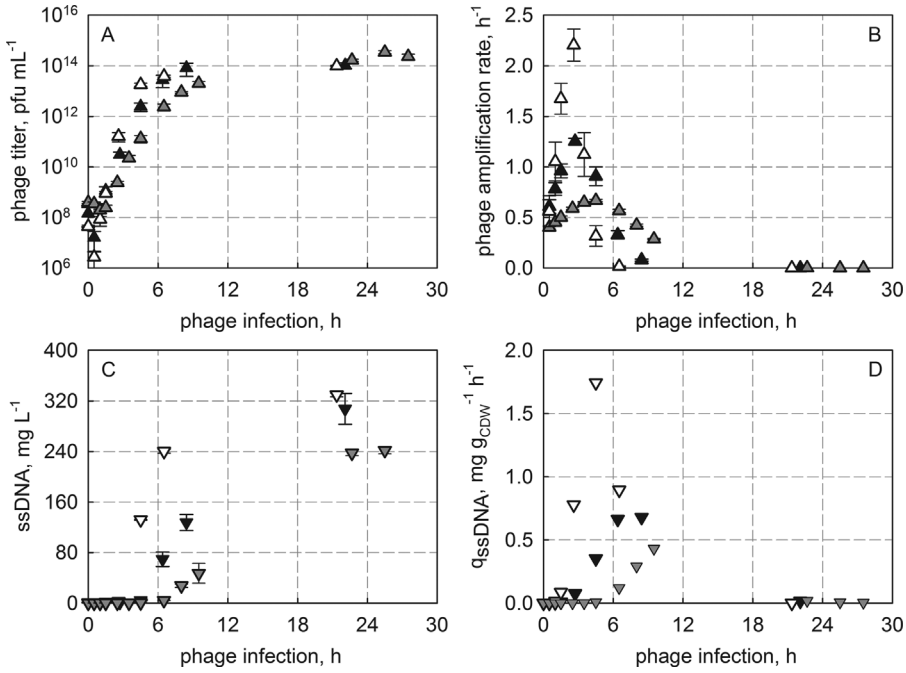

Figure 5. Phage titer and ssDNA concentrations at varying specific growth rate of *E. coli*. The fed-batch fermentations were performed with a predefined specific growth rate of $\mu_{set} = 0.2\,h^{-1}$ (white symbols), $0.15\,h^{-1}$ (black symbols), and $0.1\,h^{-1}$ (gray symbols). The corresponding feed profiles are shown in Figure 4. The phage titers (**A**), the phage amplification rates (**B**), the amount of isolated ssDNA (**C**), and the cell specific ssDNA formation rates (**D**) are shown as function of the process time after phage infection.

the same relationship. Furthermore, batch experiments are not suitable to control the specific growth rate at defined values with substrate excess.

The intracellular concentration of the replicative form of bacteriophage M13 genome is independent of the specific growth rate of the cells (Hohn et al., 1971). Considering this, the rolling circle amplification of ssDNA executed by the DNA Polymerase III of *E. coli* might be independent of growth rate and might not be the rate-determining step in phage life cycle. In contrast, the RNA polymerase and ribosome concentration has been shown to increase with increasing cell growth rate (Scott et al., 2010) and may therefore increase phage protein translation and phage amplification rate at high growth rates.

In comparison to high-cell-density fermentation for heterologous protein production, the growth and production phase are usually separated. Thus, only few publications deal with the influence of specific growth rate on protein expression in *E. coli*. Nonetheless, higher pre-induction specific growth rates have been shown to increase the productivity of alpha consensus interferon in *E. coli* (Curless et al., 1990). In the case of the production of 2-Deoxyribose-5-phosphate aldolase, higher specific growth rates have been shown to enhance the volumetric productivity (Pei et al., 2010).

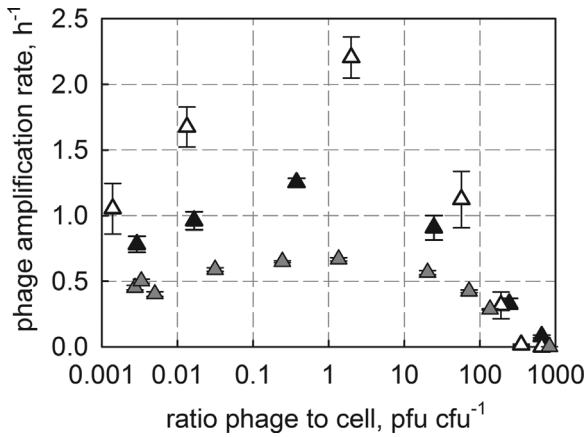

Figure 6. Phage amplification rate at different cell growth rates. The phage amplification rates are plotted against the ratio of phage to cell. The host cell growth rate was set to $\mu_{set} = 0.2\,h^{-1}$ (white symbols), $0.15\,h^{-1}$ (black symbols), and $0.1\,h^{-1}$ (gray symbols) during exponential feeding.

Variation of Multiplicity of Infection

The multiplicity of infection (MOI) represents the ratio of phage to host cell at the time of infection and was varied over a range from 0.002 to 2.3 pfu cfu^{-1}. The infection was carried out at a biomass concentration of $25\,g\,L^{-1}$ and a specific growth rate of $0.15\,h^{-1}$, since the growth rate of $0.2\,h^{-1}$ did not improve the overall ssDNA concentration. MOI of 0.002 and 0.05 pfu cfu^{-1} revealed a comparable phage titer progress with a maximal phage amplification rate of 1.3 magnitudes per hour, whereas an MOI of 2.3 led to a slower increase of the phage titer reaching a maximal phage amplification rate of 0.5 magnitudes per hour (Fig. 7A and B). Furthermore, fermentations with a MOI of $4 \cdot 10^{-7}$ resulted in a

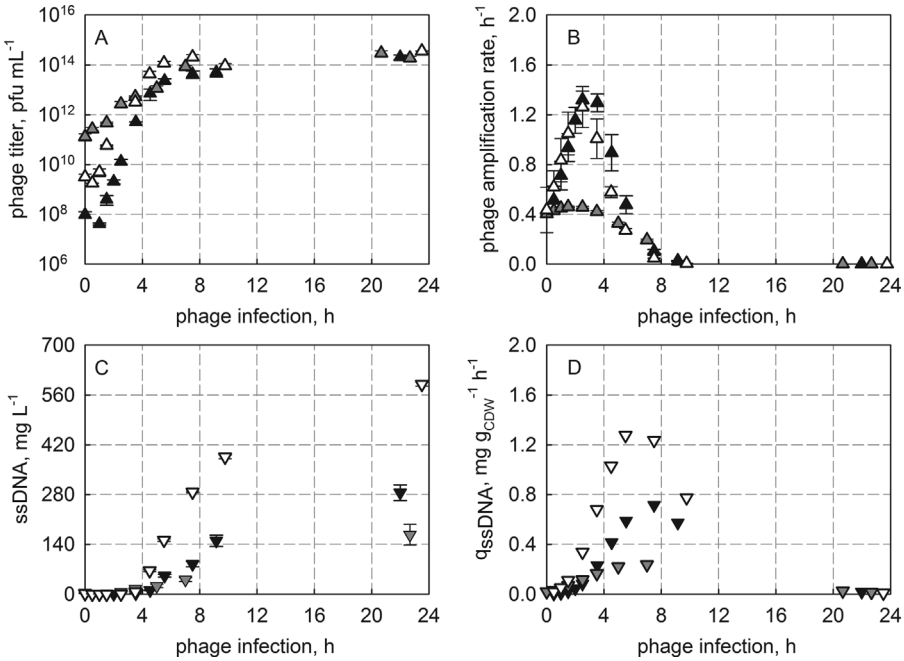

Figure 7. Influence of multiplicity of infection (MOI). Fed-batch phage fermentations were performed with MOIs of 0.002 pfu cfu^{-1} (black symbols), 0.05 pfu cfu^{-1} (white symbols), and 2.3 pfu cfu^{-1} (gray symbols). The specific growth rate during exponential feeding was set to 0.15 h^{-1}. The cells were infected after reaching a cell dry weight of 26 g L^{-1}. The phage titers (**A**), the phage amplification rates (**B**), the isolated ssDNA concentrations (**C**), and the cell specific ssDNA formation rates (**D**) are plotted against the process time after phage infection.

maximal phage amplification rate of 1.5 magnitudes per hour and maximal phage titers of $1.5 \cdot 10^{14}$ pfu mL^{-1} (data not shown in Figure 7, further data comparison see Supporting Information). Additionally, the MOI influences the produced ssDNA concentration. The highest isolated ssDNA concentration of 590 ± 5 mg L^{-1} at the end of the process was achieved with a MOI of 0.05 pfu cfu^{-1}. Accordingly, the cell specific ssDNA formation rate was enhanced up to 1.3 mg g_{CDW}^{-1} h^{-1} (Fig. 7C and D).

A high MOI of 2.3 pfu cfu^{-1} resulted in a significant reduction of phage amplification rate and correlated with the reduced adsorption rate of phage and cells at high MOI of 3–7 and maximal adsorption rate at 0.007–0.7 (Tzagoloff and Pratt, 1964). Reddy and McKenney (1996) investigated the influence of MOI between 10^{-7} and 10^{-4} pfu cfu^{-1} in batch experiments using shake flasks. They postulated that higher MOI will result in higher maximal phage titer. This finding was confirmed and extended with regard to a MOI range between 10^{-7} and $5 \cdot 10^{-2}$ in the fed-batch fermentation process. A further increase of MOI up to 2.3 pfu cfu^{-1} resulted in a lower maximal ssDNA concentration. Compared to the best so far published results, a MOI of 0.05 pfu cfu^{-1} increased the production process for scaffold M13 ssDNA by 54 % (Kick et al., 2015).

Conclusions

The characterization of the high-cell-density fermentation of *E. coli* infected with bacteriophage M13 revealed no medium limitation using defined salt medium (Riesenberg et al., 1991). The variation of time of infection during exponential growth phase (15–40 g L^{-1} CDW) had little effect on the phage amplification rate. Nevertheless, infection in the mid exponential feeding phase gave rise to higher ssDNA concentrations. In contrast, increasing the cell specific growth rate from 0.1 to 0.2 h^{-1} enhanced the phage amplification rate from 0.7 to 2.2 h^{-1}. Regarding the multiplicity of infection, an optimum value of 0.05 pfu cfu^{-1} was identified to achieve the highest final ssDNA concentration of 590 mg L^{-1} in the fed-batch process.

The improved fed-batch process discussed herein robustly provides high amounts of scaffold ssDNA that may be used for DNA origami. However, large-scale DNA origami production also requires high amounts of single-strand DNA oligonucleotides, which are currently obtained via solid-phase chemical synthesis. It will be an important task for the future to explore biotechnological methods for also producing custom DNA oligonucleotides in large amounts. In addition to uses in DNA origami, a high phage titer is useful for other areas of applications of M13, such as nanoscale electrical wiring for lithium-ion batteries (Lee et al., 2009).

This work was supported by Deutsche Forschungsgemeinschaft (DFG) through the TUM International Graduate School of Science and Engineering (IGSSE), the Excellence Cluster Center for Integrated Protein Science, Nano Initiative Munich, the Sonderforschungsbereich SFB863, and a European Research Council starting grant t256270 to Hendrik Dietz. The support of Benjamin Kick, Samantha Hensler, and Florian Praetorius by the TUM Graduate School is acknowledged as well.

Nomenclature

$c_{S,0}$	substrate concentration in feed, g L^{-1}
c_x	biomass concentration, g L^{-1}
CDW	cell dry weight, g L^{-1}

E. coli	*Escherichia coli*
μ	specific growth rate, h^{-1}
MOI	multiplicity of infection, pfu cfu^{-1}
OD_{600}	optical density at 600 nm, –
pfu	plaque forming unit
RF	replicative form
ssDNA	single-stranded DNA
t	time, h
$Y_{XS,\mu}$	biomass yield coefficient, $g\,g^{-1}$

References

Anderson RA, Nakashima Y, Coleman JE. 1975. Chemical modifications of functional residues of fd gene 5 DNA-binding protein. Biochemistry 14(5):907–917.

Berardi MJ, Shih WM, Harrison SC, Chou JJ. 2011. Mitochondrial uncoupling protein 2 structure determined by NMR molecular fragment searching. Nature 476(7358):109–113.

Bernard JML, Francis MB. 2014. Chemical strategies for the covalent modification of filamentous phage. Front Microbiol 5:734.

Blaik RA, Lan E, Huang Y, Dunn B. 2016. Gold-coated M13 bacteriophage as a template for glucose oxidase biofuel cells with direct electron transfer. ACS Nano 10(1):324–332.

Branston S, Stanley E, Ward J, Keshavarz-Moore E. 2011. Study of robustness of filamentous bacteriophages for industrial applications. Biotechnol Bioeng 108(6):1468–1472.

Branston SD, Wright J, Keshavarz-Moore E. 2015. A non-chromatographic method for the removal of endotoxins from bacteriophages. Biotechnol Bioeng 112(8):1714–1719.

Burns JR, Seifert A, Fertig N, Howorka S. 2016. A biomimetic DNA-based channel for the ligand-controlled transport of charged molecular cargo across a biological membrane. Nat Nano 11(2):152–156.

Choi JH, Keum KC, Lee SY. 2006. Production of recombinant proteins by high cell density culture of *Escherichia coli*. Biomol Eng 61(3):876–885.

Chung WJ, Oh JW, Kwak K, Lee BY, Meyer J, Wang E, Hexemer A, Lee SW. 2011. Biomimetic self-templating supramolecular structures. Nature 478(7369):364–368.

Clokie Martha RJ, Kropinski AM. 2009. Bacteriophages. Volume 1: Isolation, characterization, and interactions. Totowa, NY: Humana [u.a.]. XXII, 307 S.

Curless C, Pope J, Tsai L. 1990. Effect of preinduction specific growth rate on recombinant alpha consensus interferon synthesis in *Escherichia coli*. Biotechnol Prog 6(2):149–152.

Dimant H, Sharon N, Solomon B. 2009. Modulation effect of filamentous phage on α-synuclein aggregation. Biochem Biophys Res Commun 383(4):491–496.

Douglas SM, Bachelet I, Church GM. 2012. A logic-gated nanorobot for targeted transport of molecular payloads. Science 335(6070):831–834.

Douglas SM, Chou JJ, Shih WM. 2007. DNA-nanotube-induced alignment of membrane proteins for NMR structure determination. Proc Natl Acad Sci 104(16):6644–6648.

Douglas SM, Dietz H, Liedl T, Högberg B, Graf F, Shih WM. 2009. Self-assembly of DNA into nanoscale three-dimensional shapes. Nature 459(7245):414–418.

Ellis EL, Delbrück M. 1938. The growth of bacteriophage. J Gen Physiol 22(3):365–384.

Henry TJ, Pratt D. 1969. The proteins of bacteriophage M13. Proc Natl Acad Sci 62(3):800–807.

Hohn B, Lechner H, Marvin DA. 1971. Filamentous bacterial viruses. J Mol Biol 56(1):143–154.

Hofschneider PH. 1963. Untersuchungen über "kleine" *E. coli* K 12 bakteriophagen. Zeitschrift für Naturforschung B 18b:203–210.

Ketterer P, Willner EM, Dietz H. 2016. Nanoscale rotary apparatus formed from tight-fitting 3D DNA components. Sci Adv 2(2):e1501209.

Kick B, Praetorius F, Dietz H, Weuster-Botz D. 2015. Efficient production of single-stranded phage DNA as scaffolds for DNA origami. Nano Lett 15(7):4672–4676.

Langecker M, Arnaut V, Martin TG, List J, Renner S, Mayer M, Dietz H, Simmel FC. 2012. Synthetic lipid membrane channels formed by designed DNA nanostructures. Science 338(6109):932–936.

Lee SY. 1996. High cell-density culture of *Escherichia coli*. Trends Biotechnol 14(3):98–105.

Lee YJ, Yi H, Kim W-J, Kang K, Yun DS, Strano MS, Ceder G, Belcher AM. 2009. Fabricating genetically engineered high-power lithium-ion batteries using multiple virus genes. Science 324(5930):1051–1055.

Messing J. 2016. Phage M13 for the treatment of Alzheimer and Parkinson disease. Gene 583(2):85–89.

Moradi M, Li Z, Qi J, Xing W, Xiang K, Chiang Y-M, Belcher AM. 2015. Improving the capacity of sodium ion battery using a virus-templated nanostructured composite cathode. Nano Lett 15(5):2917–2921.

Oh J-W, Chung W-J, Heo K, Jin H-E, Lee BY, Wang E, Zueger C, Wong W, Meyer J, Kim C, Lee S-Y, Kim W-G, Zemla M, Auer M, Hexemer A, Lee S-W. 2014. Biomimetic virus-based colourimetric sensors. Nat Commun 5:3043.

Pei X, Wang Q, Qiu X, Ying L, Tao J, Xie T. 2010. The fed-batch production of a thermophilic 2-deoxyribose-5-phosphate aldolase (dera) in escherichia coli by exponential feeding strategy control. Appl Biochem Biotechnol 162(5):1423–1434.

Rakonjac J, Bennett NJ, Spagnuolo J, Gagic D, Russel M. 2011. Filamentous bacteriophage: Biology, phage display and nanotechnology applications. Curr Issues Mol Biol 13(2):51–76.

Reddy P, McKenney K. 1996. Improved method for the production of M13 phage and single-stranded DNA for DNA sequencing. Biotechniques 20(5):854.

Riesenberg D, Schulz V, Knorre WA, Pohl HD, Korz D, Sanders EA, Roß A, Deckwer WD. 1991. High cell density cultivation of *Escherichia coli* at controlled specific growth rate. J Biotechnol 20(1):17–27.

Rothemund Paul WK. 2006. Folding DNA to create nanoscale shapes and patterns. Nature 440(7082):297–302.

Salivar WO, Tzagoloff H, Pratt D. 1964. Some physical-chemical and biological properties of the rod-shaped coliphage M13. Virology 24(3):359–371.

Sambrook J, Fritsch EF, Maniatis T. 2001. Molecular cloning. A laboratory manual. Cold Spring Harbor, NY: Cold Spring Harbor Laboratory Press. Getr. Zählung.

Schröder CH, Erben E, Kaerner H-C. 1973. A rolling circle model of the in vivo replication of bacteriophage ϕX174 replicative form DNA: Different fate of two types of progeny replicative form. J Mol Biol 79(4):599–613.

Scott M, Gunderson CW, Mateescu EM, Zhang Z, Hwa T. 2010. Interdependence of cell growth and gene expression: Origins and consequences. Science 330(6007):1099–1102.

Sharma P, Ward A, Gibaud T, Hagan MF, Dogic Z. 2014. Hierarchical organization of chiral rafts in colloidal membranes. Nature 513(7516):77–80.

Shiloach J, Fass R. 2005. Growing *E. coli* to high cell density—A historical perspective on method development. Biotechnol Adv 23(5):345–357.

Stassen APM, Folmer RHA, Hilbers CW, Konings RNH. 1995. Single-stranded DNA binding protein encoded by the filamentous bacteriophage M13: Structural and functional characteristics. Mol Biol Rep 20(3):109–127.

Tzagoloff H, Pratt D. 1964. The initial steps in infection with coliphage M13. Virology 24(3):372–380.

Whaley SR, English DS, Hu EL, Barbara PF, Belcher AM. 2000. Selection of peptides with semiconductor binding specificity for directed nanocrystal assembly. Nature 405(6787):665–668.

Yan J, Hu C, Liu X, Zhong J, Sun G, He D. 2015. Recent developments of new DNA origami nanostructures for drug delivery. Curr Pharm Des 21(22):3181–3190.

Supporting Information

Additional supporting information may be found in the online version of this article at the publisher's web-site.